UNIVERSITÀ DI PARMA
ARCHIVIO DELLA RICERCA

University of Parma Research Repository

Copper Oxide Nanomaterial Fate in Plant Tissue: Nanoscale Impacts on Reproductive Tissues

note finali coverpage

(Article begins on next page)

30 January 2025

Copper Oxide nanomaterial fate in plant tissue: Nanoscale impacts on reproductive tissues

SCHOLARONE™
Manuscripts

1 **Copper Oxide nanomaterial fate in plant tissue: Nanoscale impacts on**

2 **reproductive tissues**

3 Marta Marmiroli,[1,*] Luca Pagano,[1,*] Riccardo Rossi,[1] Roberto De La Torre-Roche,[2] Giovanni Orazio

4 Lepore,[3] Roberta Ruotolo,[1] Gianluca Gariani,[4] Valentina Bonanni,[4] Simone Pollastri,[4] Alessandro

5 Puri,[5] Alessandra Gianoncelli,[4] Giuliana Aquilanti,[4] Francesco d'Acapito,[5] Jason C. White,[2,§] Nelson

6 Marmiroli[1,6,§,#]

7

8 [1] Department of Chemistry, Life Sciences and Environmental Sustainability, University of Parma, Parco Area delle

9 Scienze 11/A, 43124 Parma, Italy.

10 [2] The Connecticut Agricultural Experiment Station, 123 Huntington Street, 06504 New Haven, CT, USA.

11 [3] Earth Science Department, Univeristy of Florence, Via La Pira 4, 50121 Firenze, Italy.

12 [4] Elettra, Sincrotrone Trieste, Strada Statale 14 - km 163,5 in AREA Science Park, 34149 Trieste, Italy.

13 [5] CNR-IOM-OGG c/o ESRF – The European Synchrotron, 71 Avenue des Martyrs CS 40220, F-38043 Grenoble Cédex

14 9, France.

15 [6] Consorzio Interuniversitario Nazionale per le Scienze Ambientali (CINSA), University of Parma, 43124 Parma, Italy.

16 * co-first authorship.

17 § co-last authorship.

18 # corresponding author, nelson.marmiroli@unipr.it.

19

20 **Abstract**

21 A thorough understanding of the implications of chronic low dose exposure to Engineered

22 Nanomaterials (ENMs) through the food chain is lacking. The present study aimed to characterize

23 such response in *Cucurbita pepo* L. (zucchini) upon exposure to a potential nanoscale fertilizer:

24 copper oxide (CuO) nanoparticles. Zucchini was grown in soil amended with nano-CuO, bulk CuO

25 (100 mg Kg^{-1}) and CuSO$_4$ (320 mg Kg^{-1}) from germination to flowering (60 days). Nano-CuO

26 treatment had no impact on plant morphology or growth, nor pollen formation and viability. The

27 uptake of Cu was comparable in the plant tissues under all treatments. RNA-seq analyses on

28 vegetative and reproductive tissues highlighted common and nanoscale-specific component of the

29 response. Mitochondrial and chloroplast functions were uniquely modulated in response to

30 nanomaterial exposure as compared with conventional bulk and salt forms. X-ray Absorption

31 Spectroscopy (XAS) showed that Cu local structure changed upon nano-CuO internalization,

32 suggesting potential nanoparticles biotransformation within the plant tissues. These findings

33 demonstrate the physiological, cellular, and molecular consequences related to nano-CuO application

34 as a plant fertilizer, highlighting the differential mechanisms involved in the exposure to nano-CuO,

35 bulk or salt and the pathways of plant response to minimize environmental and health risk, through

36 sustainable nano-enabled agricultural strategies.

37

38 Keywords: nanomaterials, nanofertilization, RNA-seq, pollen, biotransformation, *Cucurbita pepo.*

39

40

41 **Synopsis**

42

43 Fertilization with nanoscale CuO affected zucchini at the physiological and molecular levels, from

44 roots to flowers, with significant internalization and particle biotransformation being evident.

45

46

47

48

49

50

51

52

53

54   **Introduction**

55

56   In recent years, interest in the utilization of nanotechnology to produce nano-enabled materials

57   and delivery platforms to address the progressive inefficiency of mineral fertilization has been rapidly

58   growing.[1,2] However, these nanomaterials are by their very nature more reactive and bioavailable than

59   traditional forms utilized in agriculture,[1-3] and as such, have raised concerns over sustainability and

60   safety with regard to human and environmental health. For example, direct utilization in agriculture

61   raises the clear possibility of food chain contamination from staple plants to humans through the

62   direct consumption of contaminated plant products as could happen with rice, maize and peanuts.[3,4]

63   In addition, the potential widespread use of engineered nanomaterials (ENMs) as part of "nano-

64   agricultural chemistry" has created concerns over damage to non-target organisms and to potential

65   trophic transfer through terrestrial food chains, through vegetables grazing by simple insects and then

66   spreading out to higher insects and predators.[5-9] As such, safety assessment and sustainability

67   evaluation must be a core component in novel materials formulations for agri-food production

68   purposes (e.g. nanopesticides, nanofertilizers). [1,10-13]

69   A number of recent studies have demonstrated the unique potential of Cu-based nanomaterials

70   in agriculture,[11,14,15] including field studies demonstrating how materials such as $Cu_3(PO4)_2$ based-

71   nanosheets and commercial CuO NPs can be foliar applied to young seedlings so as to increase plant

72   growth and suppress *Fusarium* spp. infections of tomato (*Solanum lycopersicum* L.) and watermelon

73   (*Citrullus lanatus* L.) in full life cycle studies. Furthermore, Ma *et al*. (2020)[13] studied how

74   nanomaterial chemistry could be tuned to optimize the effects of pathogen suppression and nutrient

75   release from Cu-based ENMs on sudden death syndrome (SDS) in soybean (*Glycine max* L.),

76   developing a thermodynamic model to describe how morphology and matrix effects are implicated

77   in Cu release and plant response. In addition, Cu-based nanoformulations are known to interact with

78   organic acids in plant root exudates. These interactions significantly influence ENM stability,

79   biotransformation and bioavailability,[16] as well as induce modifications in the plant metabolome.[17]

80   The role of Cu nanomaterial bioavailability has also been investigated through trophic transfer

81   experiments, including an assessment of how initial chemical form is impacted by relevant

82   weathering conditions and subsequent material transformation.[18] These findings highlight the

83   importance of controlling ENMs physico-chemical properties (e.g. morphology, composition and

84   dissolution) so as to develop safer and more sustainable nanoscale formulations for agriculture,

85   simultaneously enhancing the targeting and delivery efficiency to optimize utilization of resources

86   while minimizing negative impacts on the environment.[1]

87   The current study investigated the potential effects of CuO NPs on zucchini (*Cucurbita pepo*

88   L.) from a morphological, physiological, molecular, and atomic perspective, with a particular focus

89   on gametogenesis and pollen development. Conventional CuO bulk material and $CuSO_4$ salts were

90   used as controls to clarify nanoscale-specific effects of CuO NPs with regard to its fate within the

91   plant tissues. Particular attention was focused on the function and regulation of chloroplast and

92   mitochondrion activity, which play a critical role in pollen development. The coupling of a global

93   transcriptomic approach (by RNA-seq) with synchrotron-based analyses, such as μ-X-ray

94   Fluorescence (μ-XRF) mapping and Extended X-ray absorption fine structure (EXAFS) spectroscopy

95   of Cu states, enabled a thorough understanding of the connection between the observed biological

96   response and the physico-chemical condition of CuO NPs at a molecular and sub-molecular level in

97   different plant tissues.

98

99   **Methods**

100   *Nanomaterial characterization*

101   Copper oxide nanoparticles (CuO NPs) (99% purity; 40 nm average sized) were purchased

102   from U.S. Research Nanomaterials, Inc. (Houston, TX). Cu represents 79.8% of the total molecular

103   weight of the molecule. CuO NPs were characterized by electron microscopy (TEM, Talos F200S

104   G2, SEM FEG Thermo Fisher Scientific, Waltham, MA, USA) as reported in Figure S1. The average

105   particle size (*dh*) and zeta (ζ) potential in ddH_2O were 533.9 ± 47.2 nm and of -24.7 ± 1.4 mV as

106 determined by Zetasizer Nano Series ZS90 (Malvern Instruments, Malvern, UK), after sonication by

107 a Fisher Scientific Model 505 Sonic Dismembrator (Fisher Scientific, Waltham, MA) at 40%

108 amplitude for 60s. CuO bulk material and $CuSO_4 \cdot 5H_2O$ were purchased from Sigma Aldrich (St.

109 Louis, MO, US).

110   For particle dissolution analysis, CuO NPs and CuO bulk solutions (1000 mg L^{-1}) were

111 prepared in ddH_2O, avoiding shaking and light, and portions were collected after 1, 2, 3, 7, and 14d.

112 Aliquots of 1 ml for each sample were precipitated by ultracentrifugation at 30000 rpm, for 10 min,

113 at 20°C (Optima Max-XP Ultracentrifuge, Beckman-Coulter Inc., Brea, CA, USA). The liquid phase

114 was collected and digested in 4 mL of 1M HNO_3 (purity: 67% w/w) for 40 min at 200°C using a

115 VELP DK20 digester (VELP Scientifica, Usmate, Italy). The digests were analysed by flame atomic

116 absorption spectroscopy (FA-AAS; AA240FS, Agilent Technologies, Santa Clara, CA, USA) for the

117 presence of Cu (lamp current: 4 mA; fuel: acetylene; support: air; wavelength 324.7 nm; slit with: 0.5

118 nm; linearity of calibration, R^2: 0.9982), in three replicates. The average dissolution for CuO bulk

119 and CuO NPs were between 0.1% and 0.15%, respectively, considering the theoretical value of 100%

120 dissolution of ionic copper in $CuSO_4$.

121

122 *Plant exposure*

123   *Cucurbita pepo* L. (cv. Costata Romanesco) seeds were pre-germinated in vermiculite

124 amended with Hoagland's Solution (10%) for 10 days prior to transplanting to soil. The Cu

125 concentration administered in pre-germination was about 2 μg Kg^{-1}. Zucchini seeds were purchased

126 from Johnny's Selected Seeds (Albion, ME, USA). The experimental soil was collected from the

127 Connecticut Agricultural Experiment Station (CAES) Lockwood Farm in Hamden, CT, USA.

128 Individual solutions of CuO NPs and CuO bulk material in water (30% water capacity of

129 soil/vermiculite mixture) were probe sonicated by a Fisher Scientific Model 505 Sonic Dismembrator

130 (Fisher Scientific, Waltham, MA) at 40% amplitude for 60−120s to maximize dispersion. Solutions

131 of CuO NPs, CuO (bulk) or (copper sulfate) CuSO$_4$ were slowly added to pots containing 500g of

132 soil and manually mixed. The final concentration of NPs and bulk CuO in pots was 100 mg kg^{-1} while

133 for CuSO$_4$·5H$_2$O (copper sulfate pentahydrate), the amount was 320 mg kg^{-1}. Considering the

134 molecular weight of the single molecules taken into account, this represented a total concentration of

135 approximately 80 mg kg^{-1} for all the treatments. Additional data related to the Cu release in treated

136 soils are reported in Supporting Information (SI). The concentrations utilized were chosen to be below

137 the limit considered as potential Cu contamination in soil, and yet still able to provide information on

138 chronic plant exposure.[19-20] Furthermore, the low dose utilized and the long growth period (60 days)

139 are indicative of a chronic exposure scenario that is not common in the literature.[21] Zucchini seedlings

140 were planted (one each pot) and grown indoor under supplemental fluorescent lighting (60 μE m^2

141 sec) under a photoperiod of 16h light at approximately 22−28 °C until flowering. Plants were top

142 watered during a 60-d growth period. For all the conditions, ten biological replicates were included.

143

144 *Pollen morphology and pollen viability*

145 Alexander's staining protocol was used to test pollen viability. Free anthers were collected

146 when pollen was mature but anthers were still non-dehiscent (stage 12-13), and were fixed in

147 Carnoy's fixative (6 ethanol: 3 chloroform: 1 acetic acid) for 2h. Mature pollen was collected and

148 stained as described in Peterson *et al.* (2010).[22] After staining, all aborted and non-aborted pollen

149 grains were counted using a Zeiss Apotome 2 microscope at 20x magnification (Zeiss, Oberkochen,

150 Germany). Pollen grains were analysed fresh with no fixation or staining; they were collected from

151 mature flowers and positioned on 2 cm diameter stainless-steel sample holder (stub) covered with

152 adhesive carbon tape. An environmental scanning electron microscope (ESEM) FEG2500 FEI (FEI

153 Europe, Eindhoven, The Netherlands) operating in low-vacuum (60 Pa) with LFD (Large Field

154 Detector) was used to enable optimal Secondary Electron (SE) imaging. The cone PLA (Pressure

155 Limiting Aperture) of 500 μm improved the signal available to the Bruker X-ray detector,

156 QUANTAX XFlash. SE imaging was performed at 10 KeV with a beam size of 2.5 μm, EDX analysis

157 at 20 KeV acceleration voltage, final lens aperture of 40 μm, and beam size of 4 μm. SE images and

158 EDX spectra were collected from samples treated with CuO NPs, CuO bulk and untreated controls.

159

160 *Metal uptake measurement*

161   Flowers harvested for elemental analyses were sampled and thoroughly rinsed with tap water,

162 MilliQ water (resistivity: 18.2 MΩ cm) and 2% HNO_3 (0.01 M) to remove soil and surface-attached

163 NPs. To determine Cu content in the tissues, fresh samples were dried at 100 °C for 72 h and digested

164 in HNO_3 (purity: 67% w/w) at 115 °C, 25 min. After 30 min, 1 mL of H_2O_2 (purity: 30 % w/w) was

165 added to each digestion tube and the samples treated for an additional 30 min prior dilution to 50 mL

166 with ddH_2O. The digested samples from the 10 biological replicates per treatment were analysed by

167 inductively coupled plasma mass spectrometry (ICP-MS) Agilent 7500ce (Agilent Technologies,

168 Santa Clara, CA) for Cu presence (63 amu). The digests Cu content were quantified against a five-

169 point calibration curve based on certified reference material (SPEX CertiPrep, Metuchen, NJ, USA),

170 and that had been previously evaluated for linearity (R^2: 0.9999) and accuracy. Analytical blanks,

171 matrix blanks, and calibration verification samples were included in each sequence.

172 Roots, stems, leaves and flower biomass samples were collected after 60-d for elemental analysis.

173 Samples (10 replicates for each tissue) were digested as in the case of ICP-MS analyses and analysed

174 by Atomic Absorption Spectroscopy (AAS) (AA240FS device, Agilent Technologies, Santa Clara,

175 CA; lamp current: 4 mA; fuel: acetylene; support: air; wavelength 324.7 nm; slit with: 0.5 nm;

176 linearity of calibration, R^2: 0.9993). AAS analyses were conducted with a four-point calibration curve

177 based on standard reference material (SPEX CertiPrep, Metuchen, NJ). Biomass and Cu content in

178 all tissues were evaluated by a one-way ANOVA with a pairwise Tukey's multiple comparison test

179 (IBM SPSS v. 26.0).

180

RNA extraction and whole transcriptome analysis

181

182   RNA samples were extracted from 0.1g (fresh weight) of pollen, leaves or roots samples from

183   unamended control, CuO NP, CuO bulk and $CuSO_4$ treatments. Total RNA was extracted from 0.1 g

184   of fresh plant material using a Sigma-Aldrich Spectrum Plant Total RNA Kit (Sigma-Aldrich, St.

185   Louis, MO). Three biological replicates per treatment were used. Total RNA quality was assessed by

186   gel electrophoresis and RNA quantity was determined using a Thermo Scientific Nanodrop Lite

187   Spectrophotometer (Thermo Fisher Scientific, Wilmington, DE). Samples were sent to IGA

188   Technologies Srl (Udine, IT) for RNA sequencing service. TruSeq Stranded mRNA kit (Illumina,

189   San Diego, CA) was used for library preparation following the manufacturer's instructions. RNA

190   samples were quantified and quality tested by Agilent 2100 Bioanalyzer RNA assay (Agilent

191   Technologies, Santa Clara, CA). Final libraries were checked Agilent Bioanalyzer DNA assay

192   (Agilent Technologies, Santa Clara, CA). Libraries were prepared for sequencing and sequenced on

193   single-end 75 bp mode on NextSeq 500 (Illumina, San Diego, CA). Alignment of reads to the

194   reference transcriptome available on Cucurbitgenomics database (http://cucurbitgenomics.org/)[23]

195   was performed using STAR software with default parameters. The resulting raw data have been

196   normalized and the differentially expressed genes were identified using a 2.3 threshold of FPKM data

197   (in log2). Data have been deposited in the NCBI GEO database (accession number GSE173716).

198   A student *t* test was applied for analysis of homogeneity of variance, statistical analysis for

199   scatter plots, box and whiskers graphs. A principal component analysis (PCA) was performed with R

200   statistical   software   (www.r-project.org).   Venny   bioinformatics   tool

201   (http://bioinfogp.cnb.csic.es/tools/venny/) was used for the generation of Venn diagrams. Gene

202   Ontology (GO) analysis and *A. thaliana* ortholog gene identification was performed by the

203   Cucurbitgenomics database. The GO term enrichment analysis was conducted using a cut-off p-value

204   of 0.05 for cellular components and biological processes, and 0.03 for relevant pathways,

205   respectively. Network analysis was performed using the GeneMANIA data service

206   (http://www.genemania.org/) using *A. thaliana* orthologues genes.

207

208   *Samples preparation for synchrotron-based analyses*

209   μ-XRF and XANES analyses were performed at ELETTRA, Sincrotrone Trieste, in order to

210   analyse Cu presence and distribution in tissues; root, leaf and flower samples (0.1 g, fresh weight)

211   were cut and submerged in glutaraldehyde triphosphate in Eppendorf tubes for fixation. After three

212   days the samples were dehydrated in gradients of alcohol (from 25 to 100%) and fixed with epoxy

213   resin following Kurth et al. (2009).[24] To analyse potential variations in local structures within the

214   tissues, bulk X-ray Absorption Spectroscopy (XAS) analyses at BM08 "LISA" beamline at ESRF

215   have been performed. The protocols described in Marmiroli et al. (2020)[25] were applied. Briefly,

216   samples were mixed with pure cellulose powder (Sigma Aldrich, St. Louis, MO, USA) and pressed

217   into 1.3 cm diameter pellets using an amount of material sufficient to keep the total absorption (μ)

218   ≤1.5 above the edge.

219

220   *Low Energy μ-XRF (LE μ-XRF)*

221   μ-XRF analyses in the soft X-ray regime were performed at the TwinMic beamline at

222   ELETTRA, Sincrotrone Trieste, Italy.[26] For the present experiment, the TwinMic microscope was

223   operated in scanning transmission mode (SXM), the beam was focused on the sample through a zone

224   plate (600 μm in diameter with a 50 nm outermost zone width), and a micrometric or sub-micrometric

225   probe size was delivered. While the sample was raster-scanned perpendicularly to the incoming

226   monochromatic beam, a fast readout CCD camera collected the transmitted X-rays and an 8-silicon

227   drift detector-based XRF system acquired the emitted fluorescence photons.[27] The obtained

228   absorption and phase contrast images outline the morphological features of the sample at sub-

229   micrometer length scales, whereas the simultaneous detection of the low energy µ-XRF correlates the

230   elemental distribution to the morphology. The elemental distribution was then obtained by

231   deconvolving and fitting the XRF spectra with PyMCA software.[28] A photon energy of 1.26 keV was

232   used to excite and obtain optimal emission conditions for the elements of major interest (Cu, Na, Ni

233   and Fe) with a spot size of 1.45 µm and a dwell time of 8 s per pixel for XRF mapping and a CCD

234   dwell time of 50 ms per SXM imaging. Each map lasted approximately 5-7 h, depending on the

235   dimensions of the scanned area.

236

237   *XRF and X-ray absorption near edge structure (XANES) mapping*

238   Zucchini root and flower thin section samples were also investigated by means of XRF

239   mapping and XAS at the XRF beamline, ELETTRA Sincrotrone Trieste (Italy)[29] which covers a

240   different energy range compared to TwinMic and allows detection of heavier elements and K lines of

241   transition metals. The experiment was conducted using a Si(111) monochromator and standard

242   45º/45º geometry for fluorescence mode measurements, using an XFlash 5030 SDD (Bruker, Berlin,

243   Germany). Higher order harmonics contamination was suppressed by a pair of parallel plane mirrors

244   intercepting the beam in grazing incidence. Thin sections of samples embedded in resin were sealed

245   between two Mylar foils and fixed on the Al sample holder using a Delrin interlocking ring. This

246   design was necessary to secure the samples and to have a system compatible with the working

247   conditions of the Ultra High Vacuum Chamber (UHVC, 10^{-7} mbar) available at the XRF beamline.

248   XRF maps were collected with an incident beam energy of 10 keV and a beam size at the exit slits of

249   200x100 µm^2 (HxV) to inspect the elemental distribution. Based on the XRF maps acquired on the

250   samples (data not shown), the areas with higher content of Fe, Cu and Zn were selected to collect

251   XANES spectra at the relative K-edges. The Si(111) monochromator was calibrated before the

252   measurements using reference metal foils. All spectra were collected using 5 seconds per step and a

253   variable energy step as a function of the energy: Large step (5 eV) in the first 200 eV of the spectrum,

254   smaller step (0.2 eV) in the near-edge region and a k-constant step of 0.07 Å^{-1} further above the

255   absorption edge. Multiple spectra were collected and merged in order to increase the signal to noise

256   ratio. The oxidation state was determined using least-squares Linear Combination Fitting (LCF) based

257   on reference spectra collected on compounds of known oxidation state. Background removal,

258   normalization of XANES spectra and LCF analyses were performed using the ATHENA software

259   package.[30]

260

261   *Extended X-ray absorption fine structure (EXAFS)*

262   Extended X-ray absorption fine structure (EXAFS) measurements at the Cu K-edge (8978.9

263   eV) were performed at the LISA CRG beamline (BM08)[31] at the European Synchrotron Radiation

264   Facility (ESRF, Grenoble, France) using plant samples and three model compounds: CuO (bulk),

265   CuO NPs and $CuSO_4 \cdot 5H_2O$. The main optical features of the beamline were a fixed exit

266   monochromator with a pair of Si(111) crystals (energy resolution $\Delta E/E \approx 1.33 \cdot 10^{-4}$); Si mirrors were

267   used for harmonics rejection (E cutoff ≈ 15 KeV). Energy was calibrated with a Cu reference foil

268   (8978.9 eV). Spectra of plant samples were acquired at 80 K, in order to minimize beam-induced

269   damage, with a constant k step of 0.05 Å^{-1} up to a maximum k value of 12.5 Å^{-1}; model compounds

270   were measured at room temperature with a k step of 0.03 Å^{-1} up to k=18 Å^{-1}. Plant samples were

271   measured in fluorescence mode with a 12-element HP-Ge detector,[32] while model compounds were

272   measured in transmission mode. Multiple spectra were collected and merged in order to increase the

273   signal to noise ratio. ATHENA software[30] was used to calibrate the energy and to average multiple

274   spectra. Standard procedures were followed to extract the structural extended EXAFS signals

275   (k·χ(k)), including pre-edge background removal, spline modelling of bare atomic background, edge

276   step normalization, and energy calibration.[33] Model atomic clusters centered on the absorber atom

277   were obtained by ATOMS;[34] theoretical amplitude and phase functions were generated using the

278   FEFF8 code.[35] EXAFS spectra were fitted through the ARTEMIS software in the Fourier-Transform

279   (FT) space.[30]

280

Results and Discussion

282   *Pollen morphology and viability*

283   Pollen grain morphology was analysed by ESEM of transverse sections of developing mature

284   anthers; no overt differences were observed across treatments (Figure S2a). Pollen viability was also

285   evaluated to determine the male gametophyte developmental stage and the preservation of plant

286   reproductive fitness. Similar to morphology, there were no differences across CuO NP, CuO bulk and

287   CuSO$_4$ treatments as compared to the untreated control, with a pollen viability approximately 100%

288   in all cases (Figure S2b).

289   Previous studies have demonstrated that copper can be toxic to seed and pollen germination,

290   pollen viability and pollen tube growth; Sharafi (2014)[36] showed that high concentrations (250 mg

291   Kg^{-1}) of copper cause an almost complete inhibition of pollen germination and pollen tube

292   lengthening in almond (*Prunus dulcis* (Mill.) D.A. Webb cultivars). Similar results were observed in

293   *Pisum sativum*, where copper (35-700 mg Kg^{-1}) was highly toxic to pollen germination.[37] It is unclear

294   if zucchini exhibits a unique tolerance to copper; importantly, few studies have investigated the

295   potential effects of copper nanomaterials on pollen formation and maturation. Kumbhakar *et al.*

296   (2016)[38] showed that both copper and cadmium-based NPs reduced pollen fertility in black cumin

297   (*Nigella sativa* L.), both during pollen formation and in developmental maturation process. Similarly,

298   in *Coriandrum sativum* L. CdS NPs and CuO NPs induced physiological alterations and cytological

299   aberrations in meiotic cells, and decreased viability of pollen.[39] The alteration types and frequencies

300   in meiotic cells of *C. sativum* following NPs treatments (0.25-1 mg L^{-1}) were less severe than those

301   reported in *Nigella sativa*.[38] Notably, in the present study the Cu concentration used was specifically

302   selected to be below the limit considered for Cu contamination in soil.[19-20]

303

304   *Plant biomass and metal content*

305   After flowering, plants were harvested, and the fresh mass of roots and shoots was measured

306   (Table S1-S2). Treatment with CuO, CuO NPs and CuSO$_4$ had no impact on zucchini biomass (fresh

307   weight) compared to untreated control. These results align with much of the present literature,

308   showing that exposure to CuO NPs did not negatively impact the biological parameters in agricultural

309   crops. Tamez et al. (2019)[40] reported no significant changes in zucchini root and leaf biomass upon

310   exposure to comparable concentrations of CuO NPs. Pagano et al. (2016)[21] demonstrated that CuO

311   NPs had no effect on *C. pepo* biomass at a higher concentration (500 mg Kg^{-1}) and with an

312   experimental design that provided greater direct interaction between NPs and tissues (vermiculite

313   growth media). Alternatively, studies conducted with the model plant *Arabidopsis thaliana* grown in

314   hydroponic conditions showed a strong reduction in root length after exposure to CuO NPs (10-20

315   mg L^{-1}).[41] These contrasting results demonstrate the importance of CuO NPs dose to biological

316   response, and also highlight the influence of growth medium, plant species, and the exposure time to

317   observed effects.

318   The Cu content in soil and in the different tissues of zucchini plants was determined by Atomic

319   Absorption Spectroscopy (AAS), as shown in Table S3. The Cu content in soil was determined (14.18

320   mg Kg^{-1}) in order to justify the concentrations utilized for the experiment, highlighting a different

321   metal release percentage within the soil, starting from the same relative concentration of Cu

322   potentially available of 80 mg Kg^{-1} (salt > NP > bulk). Although there was a trend for increased Cu

323   content of tissues with all Cu treatments, only plant roots from the CuSO$_4$ exposure were significantly

324   increased. To validate the AAS results on flowers, analysis of the Cu content was performed also by

325   Inductively Coupled Plasma Mass Spectrometry (ICP-MS). Here, results show that the Cu content

326   from the CuO NPs and bulk material treatment was 43 and 30% (significant at $p < 0.05$) greater than

327   the untreated control, respectively (Table S4). This finding demonstrates that CuO NPs addition to

328   the soil does result in Cu accumulation in the reproductive tissues, although there is no difference

329   based on particle size. However, these results were impacted by instrument limits of detection (ICP-

330   MS: 0.04 μg L^{-1} vs AAS: 0.05 mg L^{-1}) and quantitation (ICP-MS: 0.1 μg mL^{-1} vs AAS: 0.1 mg L^{-1}).

331   A previous study from our group focused on zucchini exposed to nanoscale Cu evaluated a broad set

332   of physiological assays, including chlorophyll content, mitochondrial functionality, and metal content

333   in different plant tissues (roots, stems, leaves), and also demonstrated significant Cu translocation

334   from roots to both stems and leaves.[21]

335

336   *RNA-seq data analysis: critical aspects related to the CuO NP molecular response*

337   Given the evidence of an active translocation of Cu into reproductive tissues, the plant

338   transcriptomic response of different tissues and organs to exposure was evaluated using the high-

339   quality assembly of the *C. pepo* genome (NCBI BioProject PRJNA386743, sequences length 263

340   Mbps; 34240 ORFs) published on Cucurbitgenomics database.[23] Statistical analysis of RNA-seq

341   datasets showed high homogeneity between treatments in the different tissues, with comparable

342   averages and dispersions (Figures S3-S6). After normalization to the untreated control, comparison

343   across CuO NPs, CuO bulk and CuSO$_4$ exposure in roots showed 4420, 6540, and 4747 differentially

344   expressed genes in the three treatments, respectively. In leaves, the CuO NPs treatment showed a

345   lower number of differentially expressed genes compared to the other treatments: 3122 genes were

346   up- or down-regulated with CuO exposure, whereas the values for CuO bulk and CuSO$_4$ were 9924

347   and 9103, respectively. The number of differentially expressed genes in CuO NPs exposed pollen

348   was also markedly lower in comparison to the treatments in the other tissues: 1829, 2112 and 2163

349   respectively for CuO NPs, CuO bulk and CuSO$_4$ treatments. This large quantitative difference in gene

350   expression was certainly related with a larger number of different biological processes performed in

351   roots and leaves, as compared to pollen, but could be also due to the lower amount of the Cu (in

352   different forms) translocated to pollen.

353   Venn diagrams of up- and down-regulated genes in roots (Figure 1) and the relative GO

354   enrichment (Supplementary Information, SI2) data show that the transcripts in common among all

355   the tested conditions were only 4.3% and 16.3% of total genes up- and down-regulated, respectively.

356   In the roots, the specific molecular responses to the three different treatments were largely

357   independent of each other, as shown by the low percentage of gene functions common among all the

358   three conditions tested and by the two-by-two common classes. Metabolic processes and ribosome

359   translation were the most highly represented groups in biological processes related to CuO NPs and

360   CuO bulk (Figure 2; details in Supplementary Information, SI2), together with mitochondrial activity.

361   In the $CuSO_4$ treatment, unlike the NPs and bulk exposure, a nuclear component was represented,

362   and this can be related to greater Cu ion toxicity.[42] The percentage of genes commonly up- or down-

363   regulated in leaves was similar to that observed in roots: 4.7% and 16.4% total shared genes,

364   respectively (Figure 1). The percentage of genes in common between CuO bulk and $CuSO_4$ increased

365   dramatically, both for up- and down-regulated transcripts, to 40.1% and 46.6%, respectively. This

366   observation may correlate with the Cu ion release from the CuO bulk material within the plant tissues,

367   which seems to be higher than for CuO NPs, in spite of the similar dissolution rate in ddH_2O. Genes

368   involved in metabolic and energetic processes are among the more enriched genes; in addition, GO

369   terms related to chloroplast genes are well represented, as are genes for abiotic stimuli response

370   (Figure 2; details in Supplementary Information, SI3). Previous studies with *A. thaliana* highlighted

371   the role of chloroplast as a potential target of ENMs exposure.[43] Wang *et al.* (2016)[44] showed that

372   CuO NPs block electron transport between the two photosystems which can cause an excessive ROS

373   accumulation and oxidative stress, damaging biological molecules and disrupting of cellular

374   metabolism. Furthermore, CuO NPs strongly up-regulate ZAT12, a transcription factor implicated in

375   abiotic stress response, with a key role in ROS signalling pathway and co-expressed with ORF31, a

376   chloroplastic electron carrier involved in photosynthesis that has been identified as a potential

377   biomarker of ENM exposure.[21] In pollen, the percentage of genes up- or down-regulated common to

378   all treatments increased as compared to the leaves and roots: 25.5% and 33%, respectively (Figure

379   1). The percentage of genes up- and down-regulated specifically related to CuO NPs response is

380   significant (21.1% and 12.5%), when compared to the other two treatments. This data strengthens the

381   idea that CuO NPs were not only translocated (intact or modified) into the floral parts of the plant,

382   but once there, they trigger a "nanoscale-specific" response which is different from the response

383   observed in roots and leaves. These results likely reflect a multifaceted response, including partial

384   dissolution of CuO NPs and CuO bulk giving rise to a "non-specific Cu response", along with a non-

385   dissolved component exerting a nanoscale-specific response. It is also reasonable to suppose that

386   amount of Cu^{2+} derived from the three treatments increased as a consequence of the interaction with

387   plant organs and tissues.

388   Pollen has a significantly lower number of expressed genes as compared to the vegetative

389   tissues, but data highlight some pollen-specific functions and other components which have been

390   described as unique to sporophyte tissues.[45] The difference between the leaves was related to the low

391   level of expression of genes involved in energy metabolism, especially photosynthesis, since pollen

392   is not photosynthetically active. Another difference between treated and untreated plants was in

393   pollen with higher expression level of genes with functions in ion transport, cell-wall and starch

394   metabolism, and cytoskeleton dynamics (Figure 2; details in Supplementary Information, SI4).

395   Previous studies showed that polarized internal gradients and/or external fluxes of protons, potassium,

396   and chloride had a role in pollen tube function,[46] but that ion channel and transporter involvement in

397   ion fluxes across the plasma membrane in pollen tubes is still largely unknown. Starch biosynthesis

398   during the final phases of pollen maturation is fundamental because starch is a reserve source of

399   energy for pollen survival and it may also act as a metabolic checkpoint for pollen maturity. This

400   pathway is prematurely aborted whenever starch levels remain below a critical amount, strongly

401   linking pollen viability to starch deficiency.[47] A key aspect of pollen tube tip growth is the constant

402   construction of new cell wall and plasma membrane at the tube apex. Vesicles delivering this material

403   are mediated by the actin cytoskeleton.[48]

404   The whole transcriptome analysis of *C. pepo* treated with CuO NPs showed interesting

405   insights from a functional point of view. Chloroplast and mitochondrial function were critical in

406   regulating the response to CuO NPs and the energy metabolism in all plant tissues, which becomes

407   primarily mitochondrial functionality in pollen formation and development (Figure 2; details in

408   Supplementary Information, SI5). A network analysis produced for chloroplast genes in leaves, and

409   for mitochondrial genes in roots, leaves and pollen, respectively, shows the physical interactions

410   between the reported gene targets (Figures S7-S10). Genes highlighted in heatmaps and Venn

411   diagrams (Figure 3) showed a certain specificity to CuO NPs response, in particular in roots and

412   leaves. In the case of pollen, the percentage of common regulated genes among CuO NPs, CuO bulk

413   and $CuSO_4$ treatment is increased (Figure 3), suggesting that during translocation from roots to shoots

414   there was an increase in ionic Cu presence. Additional information about potential sensitive targets

415   in pollen development, derived from the study of orthologue genes in the yeast *S. cerevisiae*, were

416   investigated, highlighting a certain level of commonality in the response with the RNA-seq analyses.

417   Results are reported and described in Supplementary information (Table S5, and Figure S11).

418

419   *CuO NPs biotransformation*

420   μ-XRF analyses performed at the TwinMic beamline,[26] an example of which is depicted in

421   Figure 4, showed that in the root sections, Cu in general was mainly detectable on cell walls and more

422   visible in the treatments with $CuSO_4$, followed by nanoparticle and bulk forms where Cu content was

423   very close to TwinMic detection limits; the higher presence of Cu in the treatments with $CuSO_4$ salt

424   is due to the salt dissociation in the soil and followed by ready Cu accumulation in the roots. Notably,

425   the roots were thoroughly washed before the resin embedding procedures to avoid external

426   contamination. Fe was highly present in all root samples, including the controls, likely because it was

427   abundant in the soil. The roots maps for Cu (Figure 4a) are consistent with those obtained by Servin

428   *et al.* (2017).[18] In the flower samples (Figure 4b), it is possible to observe the pollen sacs and the

429 completely developed pollen grain; one exception is for the $CuSO_4$ treatment, where the pollen sacs

430 were noticeably smaller and possessed fewer pollen grains. Interestingly, Cu was present in the roots,

431 in particular in the cell wall, where other elements such as Ca, which is an important cofactor in

432 building of the cell wall, are known to be present.[49] In CuO bulk treatment Cu was almost not

433 detectable in roots. Although the resolution of the maps does not allow nanoparticle visualization, the

434 EXAFS analyses (Table S6, Figure 5) confirm that CuO NPs in the plants were biotransformed. This

435 suggests that cellular and molecular activities remodel and biotransform the nanoparticles. Cu was

436 present in the flowers treated with all the three types of Cu-based materials, but there were minimal

437 differences in the signal intensity and in the localization of the element. The treatment with CuO NPs

438 did not hinder formation of the flower or pollen and did not result in overt phytotoxicity, but there

439 were nanoscale-specific molecular effects at the transcriptomic levels as described by RNA-seq

440 analysis. The same was true for the bulk Cu treatment, although treatment with $CuSO_4$ did appear to

441 negatively affect gamete formation. The idea of a biotransformation of CuO NPs once within the

442 plant tissues has been reported in the literature; Servin et al. (2017) reported that after treatment,

443 transformed CuO NPs products were detected in roots as Cu_2O, Cu_2S and Cu-acetate.[18] These

444 biotransformation processes significantly influence NPs bioavailability and effects in plants,

445 including broad main metabolic and physiological processes, as well as gametogenesis.[18,50]

446   Figure 5 shows normalized XANES and EXAFS spectra of the plant samples, together with

447 those of the model compounds CuO, CuO NPs and $CuSO_4 \cdot 5H_2O$ and the EXAFS multiparameter fits.

448 Both XANES (results shown in Figure S12) and EXAFS features show that the CuO NPs structure is

449 closely related to the CuO bulk structure. EXAFS multiparameter fits (Table S6) were performed on

450 both CuO samples based on the tenorite structure,[51] yielding the same results in terms of interatomic

451 distances and path degeneracies, with both refined parameters closely agreeing with the theoretical

452 ones. EXAFS quantitative results on plant samples (Figure 5, Table S6) clearly indicate that the CuO

453 structure is not fully preserved within the plants tissues, in particular in the roots, and that after uptake,

454 the particles are biotransformed over time, leading to Cu^{2+} release starting in roots and increasing up

455   to the flower. Specifically, the prominent signal at R > 4.5 Å in the Fourier Transform (FT) spectra

456   in both CuO bulk and NPs is not visible any longer in plant samples. Moreover, the peaks at R< 4.5

457   Å are markedly weakened. In addition, no overt differences are observable among plant samples

458   treated with two different CuO types. First, shell distances in both roots and flowers are typical of

459   Cu^{2+} in square planar coordination with O and thus compatible with a remnant structure of CuO.

460   However, the Cu local environment in the higher shells shows small differences between roots and

461   flowers. Indeed, a second Cu-O shell path is systematically present in both flowers and roots at

462   significantly different distances: ≈2.7 Å in roots and 2.8 Å in flowers. Moreover, a Cu-Cu path at

463   ≈3.55 Å is always present in roots while the same path could not be fitted in flowers, the only

464   exception being plants treated with $CuSO_4$, where the path distance is much longer (3.79 Å). In shoots

465   of the Cu hyperaccumulator plant *Crassula helmsii*, Kupper at al. (2009)[52] reported Cu^{2+} O ligands

466   at 2.001 Å, indicating Cu bonds with small organic acids. Mijovilovich et al. (2009)[53] studied the

467   leaves of *Noccea caerulescences* (ecotype Ganges), an hyperaccumulator plant of Cd and Zn but

468   sensitive to Cu, reported ligands for Cu^{2+} at 1.9 Å sulfur atoms, indicating ligands with S rich

469   molecules, and at 4.5 Å, a double ligand Cu-Cu that they attributed to Cu biomineralization. These

470   findings do not align with our results and this is likely due to plant species differences;

471   hyperaccumulator plants having a unique and specific metabolic profile that is different from that of

472   non-hyperaccumulator species such as *Cucurbita pepo*.

473

474   *Environmental implications*

475   Given the essential role of Cu to the plant life cycle and its biotic response to disease, there

476   has been significant interest in its use as a potential nanofertilizer. However, in certain plants and

477   under certain concentrations, phytotoxicity has been observed. In the present study, the effect of three

478   types of Cu (CuO NPs, CuO bulk, and $CuSO_4$) was compared in *C. pepo* using a broad range of

479   physiological and molecular endpoints, with a focus on the process of male gametogenesis and pollen

480   production, which are essential to reproduction and from fruit formation and ultimately, to plant yield.

481   In a dioic species such as zucchini, gamete fertilization depends primarily on pollen quality and

482   vitality of the parental plant, which then mediates fruit production. From the morphological and

483   physiological perspective, as inferred by ESEM and XRF analyses, there were few differences

484   between the three forms of Cu (CuO NPs, CuO bulk and $CuSO_4$) in the roots, but as the Cu was

485   translocated to the flower, the $CuSO_4$ treatment exerted a more marked negative effect on pollen

486   viability. This increasing toxic response likely was a function of the complete dissolution to Cu^{2+} ions

487   in this medium and the increased reactivity of Cu in this form. Conversely, the NP form exerted

488   almost no effects on pollen and exhibited a reduced stimulation of Cu uptake, possibly being a

489   function of Cu complexed to organic ligands within the plant tissues that mitigated chemical

490   dissolution. The CuO bulk material results for the molecular and physiological endpoints were more

491   similar to $CuSO_4$, in spite of the CuO bulk and CuO NPs dissolution behavior in ddH_2O being quite

492   similar. Interesting, some nanoscale materials release ions at a greater rate than bulk materials, due

493   to increased surface area and volume.[14] However, coatings, complexation and corona formation could

494   modulate dissolution. The transcriptomic analysis of the different tissues and flowers showed that

495   metabolic processes and ribosome translation were highly represented among the most responsive

496   pathways. Chloroplast and especially mitochondrial functions were particularly affected in response

497   to CuO NPs, which agrees with previous data and aligns with the organelle's role in energy

498   metabolism in all plant tissues,[44] and specifically in pollen formation and development. In addition,

499   the EXAFS features demonstrate the occurrence of CuO NPs biotransformation, highlighting a

500   similar Cu local environment from roots to flowers. The similarity of the Cu environment after

501   different treatments seemed to depend more on the plant tissue than on the type of treatment,

502   suggesting that the biotransformed Cu environment is reached after substantial dissolution of Cu ions,

503   followed by stabilization of Cu in complexes whose nature is more dependent on the plant

504   characteristics than on the type of treatment. Indeed, the transcriptomic data showed that at the

505   molecular level, the response was partially nanoscale-specific, including in the pollen. Similar

506   phenomena have been reported for other nanomaterials such as CeO_2 NPs and CdS QDs.[25,54] The

507   evidence for the formation of Cu ions when CuO NPs are accumulated by the plants and the fact that

508   still there is a certain level of nanoscale-specific response suggests that *in planta* biotransformation

509   processes are significant and critical to overall plant response. Overall, this suggests nanoscale CuO

510   NPs as nanofertilizers likely presents minimal concerns to general plant health. A thorough and

511   mechanistic understanding of these processes such as that provided by this study will be necessary to

512   ensure the safe and sustainable application of Cu-based and other nanoscale materials in nano-enabled

513   agricultural strategies.

514

515

525

526   **Authors contribution**

527   MM, LP, NM and JCW coordinated the study and designed the experiments. RR, LP and RD

528   performed individual experiments and analysed the physiological and molecular data in with

529   collaboration of MM and RRu. AG, GA, performed the synchrotron analyses in Trieste with

530   collaboration of SP, GG and VB. AP, FA and GOL (remotely) performed the XAS measurements at

531   LISA BM08 beamline at ESRF; GOL performed EXAFS data analysis in collaboration with FA. All

532   authors contributed to manuscript revision and approved the final version.

533

Conflict of interest

535   The authors declare no conflict of interest.

536

537

Supplementary Information (SI) description:

539   *Supplementary information included* (SI1):

540   Method section and results for qPCR of genes involved in gametogenesis

541   Results of LCF analysis of XANES spectra

542   Figure S1: CuO nanoparticles visualization by TEM

543   Figure S2: ESEM micrographs pollen grains and pollen viability assay

544   Figure S3: Statistics of the genes datasets from roots samples

545   Figure S4: Statistics of the genes datasets from leaves samples

546   Figure S5: Statistics of the genes datasets from pollen samples

547   Figure S6: PCA of all data profiles

548   Figure S7: Gene network of chloroplast targets observed in leaves treated with CuO NPs

549   Figure S8: Gene network of mitochondrial targets observed in roots treated with CuO NPs

550   Figure S9: Gene network of mitochondrial targets observed in leaves treated with CuO NPs

551   Figure S10: Gene network of mitochondrial targets observed in pollen treated with CuO NPs

552   Figure S11: Heatmap transciprotmics genes involved in meiosis and gametogenesis

553   Figure S12: XANES fits and relative K-edge data

554   Table S1: Biomass of roots and shoots

555   Table S2: Flower biomass

556   Table S3: Copper concentration measured in soil, roots, shoots and flowers by AAS

557   Table S4: Copper concentration measured in flowers by ICP-MS

558   Table S5: Genes' information and primer sequences utilized in Real time PCR assay

559   `Table S6: EXAFS multiparameter fit details for studied samples and`

560   `reference compounds`

561

562   *Supplementary information reported in excel format:*

563   Supplementary Information 2 (SI2): GO analysis of up- and down-regulated genes exposed to CuO

564   NPs, CuO bulk and $CuSO_4$ in roots.

565   Supplementary Information 3 (SI3): GO analysis of up- and down-regulated genes exposed to CuO

566   NPs, CuO bulk and $CuSO_4$ in leaves.

567   Supplementary Information 4 (SI4): GO analysis of up- and down-regulated genes exposed to CuO

568   NPs, CuO bulk and $CuSO_4$ in pollen.

569   Supplementary Information 5 (SI5): *A. thaliana* ortholog genes analysis of relevant chloroplast and

570   mitochondrial targets isolated from *C. pepo* exposed to CuO NPs, CuO bulk and $CuSO_4$ in roots,

571   leaves and pollen.

572

573

574   **References**

575

576   1. Lowry, G. V., Avellan, A., Gilbertson, L. M. Opportunities and challenges for

577   nanotechnology in the agri-tech revolution. *Nat. Nanotechnol*., **2019**, 14, 17–522.

578   2. Adisa, I.; Pullagurala, V.L.R.; Peralta-Videa, J.R.; Dimkpa, C.O.; Ma, C.; Elmer, W.H.;

579   Gardea-Torresdey J.L.; White, J.C. **2019**. Recent advances in nano-enabled fertilizers and

580   pesticides: A critical review of mechanisms of action. *Environ. Sci.: Nano*. 6, 2002.

581   3. Dimkpa, C.O., Bindraban, P.S. Nanofertilizers: New Products for the Industry? *J Agric Food

582   Chem*. **2018**, 66(26), 6462-6473. doi: 10.1021/acs.jafc.7b02150.

583   4. Rui, M.; Ma, C.; White, J.C.; Tang, X.; Yang, J.; Jiang, F.; Hao, Y.; Ali, A.; Rui, Y.; Cao, W.;

584   Xing, B. Metal oxide nanoparticles alter peanut (Arachis hypogaea L.) physiological response

585   and reduce nutritional quality: A life cycle study. *Environ. Sci.: Nano*. **2018**, 5, 2088-2102.

586   5. Keller, A.A.; McFerran, S.; Lazareva, A.; Suh, S. Global life cycle releases of engineered

587   nanomaterials. *J. Nanopart. Res.*, **2013**, 15, 1692−1709.

588   6. Gardea-Torresdey, J.L.; Rico, C.M.; White, J.C. Trophic transfer, transformation, and impact

589   of engineered nanomaterials in terrestrial environments. *Environ. Sci. Technol.*, **2014**, 48,

590   2526–2540.

591   7. Hawthorne, J.; De la Torre Roche, R.; Xing, B.; Newman, L.A.; Ma, X.; Majumdar, S.;

592   Gardea-Torresdey, J.; White, J.C. Particle-size dependent accumulation and trophic transfer

593   of cerium oxide through a terrestrial food chain. *Environ. Sci. Technol.* **2014**, 48, 13102-

594   13109.

595   8. Ma, C.; White, J.C.; Zhao, J.; Zhao, Q.; Xing, B. Uptake of Engineered Nanoparticles by Food

596   Crops: Characterization, Mechanisms, and Implications. *Annu. Rev. Food Sci. Technol.* **2018**,

597   9, 129–53.

598   9. Majumdar, S.; Ma, C.; Villani, M.; Zuverza-Mena, N.; Pagano, L.; Huang, Y.; Zappettini, A.;

599   Keller, A.A.; Marmiroli, N.; Dhankher, O.P.; White, J.C. Surface coating determines the

600   response of soybean plants to cadmium sulfide quantum dots. *NanoImpact*, **2019**, 14, 100151.

601   Doi: 10.1016/j.impact.2019.100151.

602   10. Servin, A. D.; White, J. C. Nanotechnology in agriculture: Next steps for understanding

603   engineered nanoparticle exposure and risk. *NanoImpact*. **2016**, 1, 9−12.

604   11. Elmer, W.; De la Torre-Roche, R.; Pagano, L.; Majumdar, S.; Zuverza-Mena, N.; Dimkpa,

605   C.; Gardea-Torresdey, J.; White, J. C. Effect of metalloid and metallic oxide nanoparticles on

606   Fusarium wilt of watermelon. *Plant Dis.* **2018**, 102 (7), 1394−1401.

607   12. Kah, M.; Tufenkji, N.; White, J.C. Nano-enabled strategies to enhance crop nutrition and

608   protection. *Nat. Nanotechnol.*, **2019**, 14, 532–540.

609   13. Ma, C.; Borgatta, J.; Hudson, B.G.; Abbaspour-Tamijani, A.; De La Torre-Roche, R; Zuverza-

610   Mena N.; Shen, Y.; Elmer, W.; Xing, B.; Mason, S.E.; Hamers, R.J. White J.C. Advanced

611   material modulation of nutritional and phytohormone status alleviates damage from soybean

612   sudden death syndrome. *Nat. Nanotechnol.* **2020**. Doi: 10.1038/s41565-020-00776-1.

613   14. Borgatta, J.; Ma, C.; Hudson-Smith, N.; Elmer, W.; Plaza Perez, C.D.; De La Torre-Roche,

614   R.; Zuverza-Mena, N.; Haynes, C.L.; White, J.C.; Hamers, R.J. Copper Based Nanomaterials

615   Suppress Root Fungal Disease in Watermelon (Citrullus lanatus): Role of Particle

616   Morphology, Composition and Dissolution Behavior. *ACS Sus Chem Eng* **2018,** 6 (11),

617   14847-14856. Doi: 10.1021/acssuschemeng.8b03379

618   15. Ma, C.; Borgatta, J.; De La Torre-Roche, R.; Zuverza-Mena, N.; White, J.C.; Hamers, R.J;

619   Elmer, W. Time-Dependent Transcriptional Response of Tomato (Solanum lycopersicum L.)

620   to Cu Nanoparticle Exposure upon Infection with Fusarium oxysporum f. sp. Lycopersici.

621   *ACS Sus Chem Eng* **2019,** 7 (11), 10064-10074. Doi: 10.1021/acssuschemeng.9b01433.

622   16. Huang Y.; Zhao, L.; Keller, A.A. Interactions, Transformations, and Bioavailability of Nano-

623   Copper Exposed to Root Exudates. *Environ Sci Technol.*, **2017** 51 (17), 9774-9783. Doi:

624   10.1021/acs.est.7b02523.

625   17. Huang, Y.; Li, W.; Minakova, A.S.; Anumol, T.; Keller, A.A. Quantitative analysis of changes

626   in amino acids levels for cucumber (*Cucumis sativus*) exposed to nano copper. *NanoImpact*,

627   **2018**, 12, 9-17. doi: 10.1016/j.impact.2018.08.008.

628   18. Servin, A.D.; Pagano, L.; Castillo-Michel, H.; De la Torre-Roche, R.; Hawthorne, J.;

629   Hernandez-Viezcas, J.A.; Loredo-Portales, R.; Majumdar, S.; Gardea-Torresdey, J.L.;

630   Dhankher, O.P.; White, J.C. Weathering in soil increases nanoparticle CuO bioaccumulation

631   within a terrestrial food chain. *Nanotoxicology*, **2017**, 11, 98–111. Doi:

632   10.1080/17435390.2016.1277274.

633   19. McLean, E.J.; Bledsoe, B.E. Behavior of Metals in Soils. *United States Environmental*

634   *Protection Agency*, **1992**, EPA/540/S-92/018.

635   20. Shabbir, Z.; Sardar, A.; Shabbir, A.; Abbas, G.; Shamshad, S.; Khalid, S.; Natasha; Murtaza,

636   G.; Dumat, C.; Shahid, M. Copper uptake, essentiality, toxicity, detoxification and risk

637   assessment in soil-plant environment. *Chemosphere*, **2020**, 259, 127436.

638   21. Pagano, L.; Servin, A. D.; De La Torre-Roche, R.; Mukherjee, A.; Majumdar, S.; Hawthorne,

639   J.; Marmiroli, M.; Maestri, E.; Marra, R. E.; Isch, S. M.; Dhankher, O. P.; White, J. C.;

640   Marmiroli, N. Molecular Response of Crop Plants to Engineered Nanomaterials. *Environ. Sci.*

641   *Technol.* **2016**, *50* (13), 7198–7207. Doi: 10.1021/acs.est.6b01816.

642   22. Peterson, R.; Slovin, J. P.; Chen, C. A Simplified Method for Differential Staining of Aborted

643   and Non-Aborted Pollen Grains. *Int. J. Plant Biol.* **2010**, 1 (2), 66–69. Doi:

644   10.4081/pb.2010.e13.

645   23. Montero-Pau, J.; Blanca, J.; Bombarely, A.; Ziarsolo, P.; Esteras, C.; Martí-Gómez, C.;

646   Ferriol, M.; Gómez, P.; Jamilena, M.; Mueller, L.; Picó, B.; Cañizares, J. De Novo Assembly

647   of the Zucchini Genome Reveals a Whole-Genome Duplication Associated with the Origin

648   of the Cucurbita Genus. *Plant Biotechnol. J.* **2018**, *16* (6), 1161–1171. Doi:

649   10.1111/pbi.12860.

650   24. Kurth, T.; Weiche, S.; Vorkel, D.; Kretschmar, S.; Menge, A. Histology of plastic embedded

651   amphibian embryos and larvae. *Genesis*. **2012**, 50, 235-250. doi:10.1002/dvg.20821.

652   25. Marmiroli, M.; Lepore, G.O.; Pagano, L.; d'Acapito, F.; Gianoncelli, A.; Villani, M.;

653   Lazzarini, L.; White, J.C.; Marmiroli, N. The fate of CdS Quantum Dots in plants as revealed

654   by Extended X-ray Absorption Fine Structure (EXAFS) analysis. *Environ. Sci.: Nano*, **2020**.

655   Doi: 10.1039/C9EN01433K.

656   26. Gianoncelli, A., Kourousias, G., Merolle, L., Altissimo, M. & Bianco, A. Current status of

657   the TwinMic beamline at Elettra: a soft X-ray transmission and emission microscopy station.

658   *J. Synchrotron Rad*. **2016**, 23, 1526-1537. doi: 10.1107/S1600577516014405.

659   27. Gianoncelli, A.; Castaing, J.; Bouquillon, A.; Polvorinos, A.; Walter, P. Quantitative

660   elemental analysis of Della Robbia glazes with a portable XRF spectrometer and its

661   comparison to PIXE methods. *X-Ray Spectrom.*, **2006**. 35: 365-369. doi:10.1002/xrs.920.

662   28. Solé, V.; Papillon, E.; Cotte, M.; Walter, P.; Susini, J. A Multiplatform Code for the Analysis

663   of Energy-Dispersive X-ray Fluorescence Spectra. *Spectrochimica Acta Part B: Atomic*

664   *Spectroscopy*. **2007**. 62. 63-68. Doi: 10.1016/j.sab.2006.12.002.

665   29. Karydas, A.; Czyzycki, M.; Leani, J.; Migliori, A.; Osan, J.; Bogovac, M.; Wrobel, P.; Vakula,

666   N.; Padilla A.R.; Menk, R.H.; Gol, M.; Antonelli, M.; Tiwari, M.; Caliri, C.; Vogel-Mikus,

667   K.; Darby, I. An IAEA multi-technique X-ray spectrometry endstation at Elettra Sincrotrone

668   Trieste: benchmarking results and interdisciplinary applications. *J. Synchrotron Radiation*.

669   **2017**. 25. 189. 10.1107/S1600577517016332.

670   30. Ravel, B.; Newville, M. ATHENA and ARTEMIS: Interactive graphical data analysis using

671   IFEFFIT. *Phys. Scr.* **2006**, 115, 1007-1010. Doi: 10.1238/Physica.Topical.115a01007.

672   31. d'Acapito, F., Lepore, G.O., Puri, A., Laloni, A., La Mannna, F., Dettona, E., De Luisa, A.,

673   Martin, A. The LISA beamline at ESRF. *J. Synchrotron Radiat.* **2019**, 26, 551-558.

674   32. Puri, A.; Lepore, G. O.; d'Acapito, F. The New Beamline LISA at ESRF: Performances and

675   Perspectives for Earth and Environmental Sciences. *Condens Matter* **2019**, 4, 12-19.

676   33. Lee, P. A.; Citrin, P. H.; Eisenberger, P. T.; Kincaid, B. M. Extended x-ray absorption fine

677   structure - its strengths and limitations as a structural tool. *Rev Mod Phys* **1981**, 53, 769-806.

678   34. Ravel, B. ATOMS: crystallography for the X-ray absorption spectroscopist. J Synchr Rad

679   **2001** 8, 314–316.

680   35. Ankudinov, A.L.; Ravel, B.; Rehr, J.J.; Conradson, S.D. Real-space multiple-scattering

681   calculation and interpretation of x-ray-absorption near-edge structure. *Phys Rev B* **1998**, 58,

682   7565-7576.

683   36. Sharafi, Y. Effects of Copper and Leadon Pollen Germination Traits in Almond Cultivars. *J.*

684   *Nuts Relat. Sci.* **2014**, *5* (2), 67–73.

685   37. Sabrine, H.; Afif, H.; Mohamed, B.; Hamadi, B.; Maria, H. Effects of Cadmium and Copper

686   on Pollen Germination and Fruit Set in Pea (Pisum Sativum L.). *Sci. Hortic.* **2010**, *125* (4),

687   551−555. doi: 10.1016/j.scienta.2010.05.031.

688   38. Kumbhakar, D. V.; Datta, A. K.; Mandal, A.; Das, D.; Gupta, S.; Ghosh, B.; Halder, S.; Dey,

689   S. Effectivity of Copper and Cadmium Sulphide Nanoparticles in Mitotic and Meiotic Cells

690   of Nigella Sativa L. (Black Cumin) – Can Nanoparticles Act as Mutagenic Agents? *J. Exp.*

691   *Nanosci.* **2016**, *11* (11), 823−839. Doi: 10.1080/17458080.2016.1149236.

692   39. Pramanik, A.; Datta, A. K.; Das, D.; Kumbhakar, D. V.; Ghosh, B.; Mandal, A.; Gupta, S.;

693   Saha, A.; Sengupta, S. Assessment of Nanotoxicity (Cadmium Sulphide and Copper Oxide)

694   Using Cytogenetical Parameters in Coriandrum Sativum L. (Apiaceae). *Cytol. Genet.* **2018**,

695   *52* (4), 299−308. Doi: 10.3103/S0095452718040084.

696   40. Tamez C, Hernandez-Molina M, Hernandez-Viezcas J.A, Gardea-Torresday J.L. Uptake,

697   transport, and effects of nano-copper exposure in zucchini (Cucurbita pepo). *Sci Total*

698   *Environ.* **2019**, 665, 100-106. Doi: 10.1016/j.scitotenv.2019.02.029

699   41. Tang, Y.; He, R.; Zhao, J.; Nie, G.; Xu, L.; Xing, B. Oxidative Stress-Induced Toxicity of

700   CuO Nanoparticles and Related Toxicogenomic Responses in Arabidopsis Thaliana. *Environ.*

701   *Pollut.* **2016**, *212*, 605−614. Doi: 10.1016/j.envpol.2016.03.019.

702   42. Dutta, S.; Mitra, M.; Agarwal, P.; Mahapatra, K.; De, S.; Sett, U.; Roy, S. Oxidative and

703   Genotoxic Damages in Plants in Response to Heavy Metal Stress and Maintenance of Genome

704   Stability. *Plant Signal. Behav.* **2018**, *13* (8), 1−17. Doi: 10.1080/15592324.2018.1460048.

705   43. Ruotolo, R.; Maestri, E.; Pagano, L.; Marmiroli, M.; White, J. C.; Marmiroli, N. Plant

706   Response to Metal-Containing Engineered Nanomaterials: An Omics-Based Perspective.

707   *Environ. Sci. Technol.* **2018**, *52* (5), 2451−2467. Doi: 10.1021/acs.est.7b04121.

708   44. Wang, Z.; Xu, L.; Zhao, J.; Wang, X.; White, J. C.; Xing, B. CuO Nanoparticle Interaction

709   with Arabidopsis Thaliana: Toxicity, Parent-Progeny Transfer, and Gene Expression.

710   *Environ. Sci. Technol.* **2016**, *50* (11), 6008−6016. Doi: 10.1021/acs.est.6b01017.

711   45. Honys, D.; Twell, D. Comparative Analysis of the Arabidopsis Pollen Transcriptome. *Plant*

712   *Physiol.* **2003**, *132* (June), 640–652. Doi: 10.1104/pp.103.020925.

713   46. Hepler, PK; Vidali, L; Cheung, AY. Polarized cell growth in higher plants. *Annual Rev. Cell.*

714   *Dev. Biol. **2001**,* 17: 159–187

715   47. Wen, L. Y.; Chase, C. D. Mitochondrial Gene Expression in Developing Male Gametophytes

716   of Male-Fertile and S Male-Sterile Maize. *Sex. Plant Reprod.* **1999**, *11* (6), 323–330. Doi:

717   10.1007/s004970050159.

718   48. Da Costa-Nunes, J. A.; Grossniklaus, U. Unveiling the Gene-Expression Profile of Pollen.

719   *Genome Biol.* **2003**, *5* (1), 9–11. Doi: 10.1186/gb-2003-5-1-205.

720   49. Hepler P.K. Calcium: A Central Regulator of Plant Growth and Development. *The Plant Cell*.

721   **2005**, 17(8) 2142-2155. Doi: 10.1105/tpc.105.032508.

722   50. Dai, Y.; Zhao, J.; Liu, X.; Yu, X.; Jiang, Z.; Bu, Y.; Xu, Z.; Wang, Z.; Zhu, X.; Xing, B.

723   Transformation and Species Identification of CuO Nanoparticles in Plant Cells (Nicotiana

724   Tabacum). *Environ. Sci. Nano* **2019**, *6* (9), 2724–2735. Doi: 10.1039/c9en00781d.

725   51. Wyckoff, R. W. G. Crystal Structures 1963. 1, 85–237. Second edition. Interscience

726   Publishers, New York.

727   52. Küpper, H.; Götz, B.; Mijovilovich, A.; Küpper, F.C.; Meyer-Klaucke, W. Complexation and

728   Toxicity of Copper in Higher Plants. I. Characterization of Copper Accumulation, Speciation,

729   and Toxicity in *Crassula helmsii* as a New Copper Accumulator. *Plant. Physiol.* **2009**, 151

730   (2) 702-714. Doi: 10.1104/pp.109.139717.

731   53. Mijovilovich, A.; Leitenmaier, B.; Meyer-Klaucke, W.; Kroneck, P.M.H.; Götz, B.; Küpper,

732   H. Complexation and Toxicity of Copper in Higher Plants. II. Different Mechanisms for

733   Copper versus Cadmium Detoxification in the Copper-Sensitive Cadmium/Zinc

734   Hyperaccumulator *Thlaspi caerulescens* (Ganges Ecotype). *Plant. Physiol.* **2009,** 151 (2),

735   715–731. Doi/10.1104/pp.109.144675.

736   54. Servin, A.D.; De la Torre-Roche, R.; Castillo-Michel, H.; Pagano, L.; Hawthorne, J.;

737   Musante, C.; Pignatello, J.; Uchimiya, M.; White, J.C. Exposure of agricultural crops to

738   nanoparticle CeO_2 in biochar-amended soil. *Plant Physiol. Biochem*., **2017**, 110, 147-157.

739   Doi: 10.1016/j.plaphy.2016.06.003.

740

741

742   **Figure captions:**

743   Figure 1. Comparison of high-throughput transcriptional datasets related to the molecular response

744   of *C. pepo* in condition of treatment with CuO NPs, CuO bulk and $CuSO_4$, in the roots (a), leaves (b),

745   pollen (c), represented with Venn diagrams. Up-regulated and down-regulated genes are reported on

746   left and right side, respectively. Percentage of identity between CuO NPs, CuO bulk and $CuSO_4$ is

747   also reported. Data were normalized on the untreated controls, with a 2.3 threshold of raw data (in

748   log2). Data highlighted an increase in the percentage of common genes involved in the response to

749   the three different Cu-based forms from roots to pollen, suggesting an increased bioavailability of

750   free Cu in the plant shoots.

751

752   Figure 2. GO biological processes expressed in percentage (%) of gene cluster enriched, related to

753   roots (a), leaves (b), and pollen (c) related to the treatment with 100 mg kg^{-1} of CuO NPs. Up-

754   regulated and down-regulated genes are reported as blue and orange bars, respectively. Additional

755   details related to GO analyses in the different tissues are available in Supplementary Information,

756   SI2-SI4.

757

758   Figure 3. Heatmaps and Venn diagrams comparison of the genes involved in chloroplast functions in

759   response to CuO NPs, CuO bulk and CuSO$_4$, in leaves (a), and in mitochondrial functions identified

760   in roots (b), leaves (c) and pollen (d) tissues. Data related to the specific genes are reported in

761   Supplementary Information, SI5. Data confirmed the increase in percentage of common modulated

762   genes from roots to pollen in response to the three different Cu-based forms utilized for the treatments.

763

764   Figure 4. μ-XRF maps of (a) roots and (b) flowers from plants treated with CuO NPs. Names of the

765   mapped elements are on top of each figure. The maps are related to the black and white square on top

766   left (Abs) which is the 20x image of the cells in the root tissue and pollen sac tissues treated with

767   CuO NPs. Cu map is always the last in the second row for (a) and (b).

768

769   Figure 5. XANES spectra of the measured samples and model compounds (a). Cu K-edge k^2-weighted

770   EXAFS region (b) and Fourier transforms (c) of plant tissues and model compounds. Solid lines are

771   data, red lines are fits. Energy was calibrated with a Cu reference foil (8978.9 eV). In order to

772   minimize beam-induced damage, spectra of samples were acquired at 80 K with a constant k step of

773   0.05 Å^{-1} up to a maximum k value of 12.5 Å^{-1} for plant tissues while model compounds were measured

774   at room temperature with a k step of 0.03 Å^{-1} up to k=18 Å^{-1}. Plant samples were measured in the
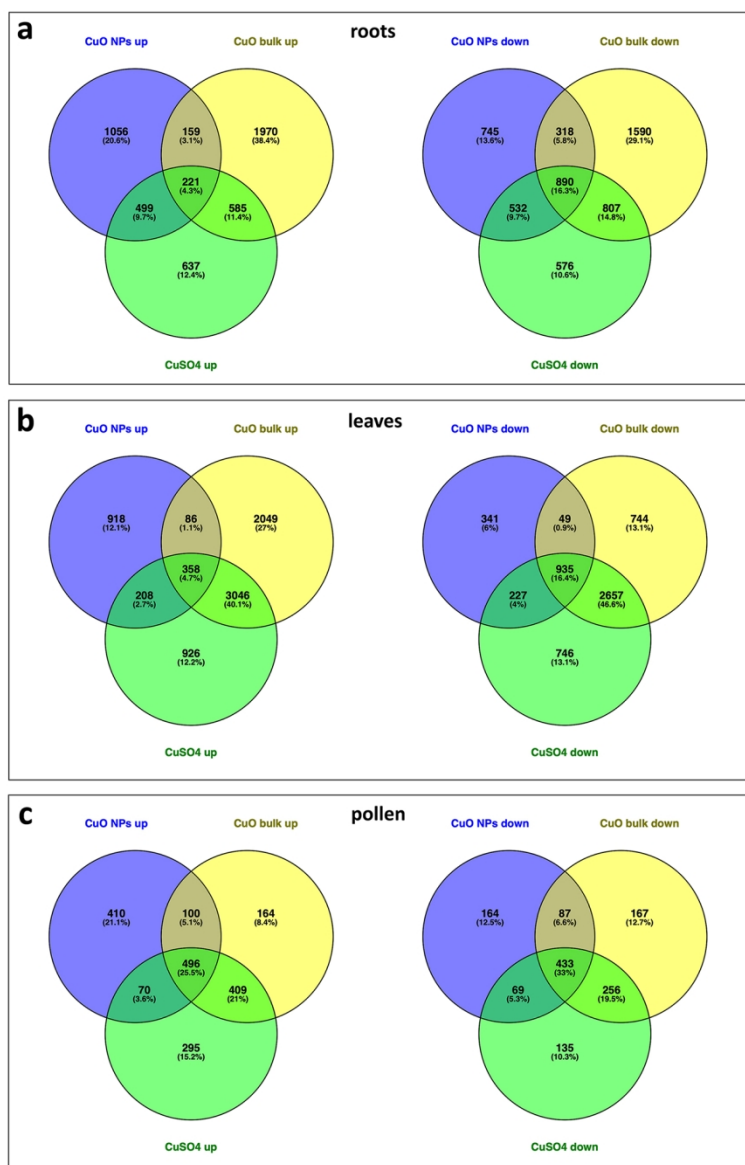
775   fluorescence mode with a 12-element HP-Ge detector.

Figure 1. Comparison of high-throughput transcriptional datasets related to the molecular response of C. pepo in condition of treatment with CuO NPs, CuO bulk and CuSO4, in the roots (a), leaves (b), pollen (c), represented with Venn's diagrams. Up-regulated and down-regulated genes are reported on left and right side, respectively. Percentage of identity between CuO NPs, CuO bulk and CuSO4 is also reported. Data were normalized on the untreated controls, with a 2.3 threshold of raw data (in log2). Data highlighted an increase in the percentage of common genes involved in the response to the three different Cu-based forms from roots to pollen, suggesting an increased bioavailability of free Cu in the plant shoots.
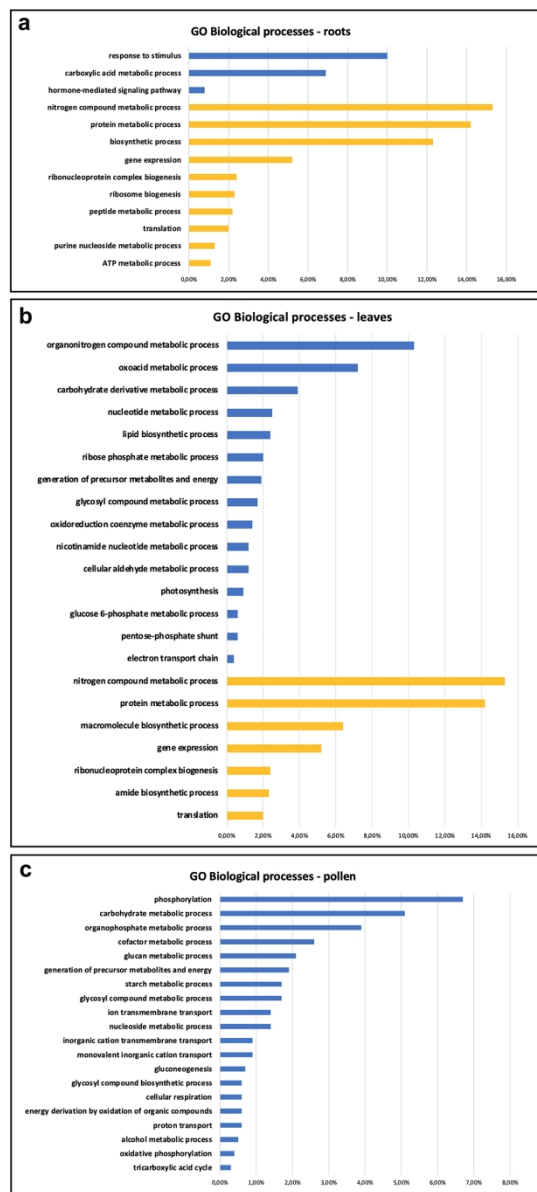
Figure 2. GO biological processes expressed in percentage (%) of gene cluster enriched, related to roots (a), leaves (b), and pollen (c) related to the treatment with 100 mg kg-1 of CuO NPs. Up-regulated and down-regulated genes are reported as blue and orange bars, respectively. Additional details related to GO analyses in the different tissues are available in Supplementary Information, SI2-SI4.
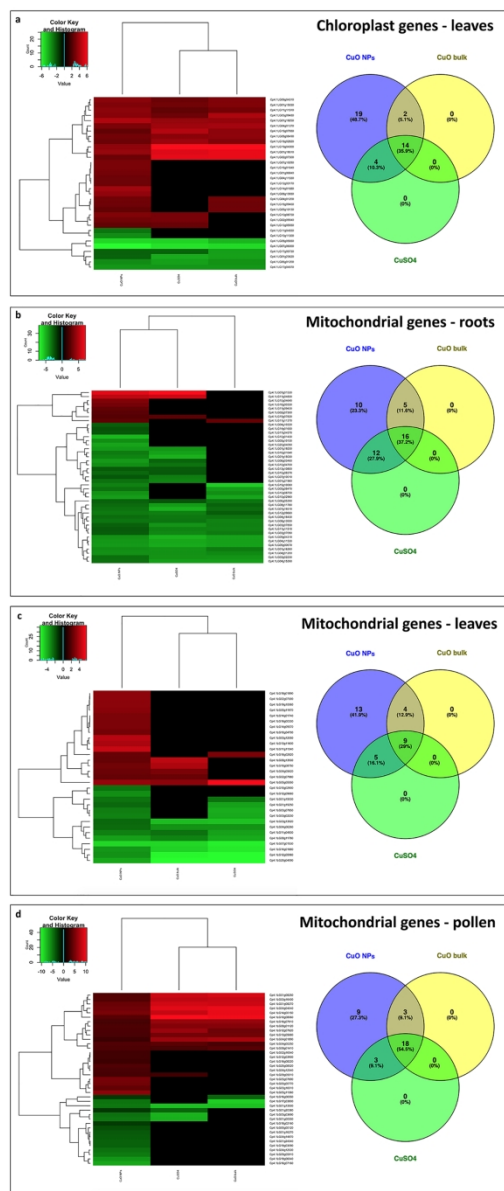
101x223mm (300 x 300 DPI)

Figure 3. Heatmaps and Venn's diagrams comparison of the genes involved in chloroplast functions in response to CuO NPs, CuO bulk and CuSO4, in leaves (a), and in mitochondrial functions identified in roots (b), leaves (c) and pollen (d) tissues. Data related to the specific genes are reported in Supplementary Information, SI5. Data confirmed the increase in percentage of common modulated genes from roots to pollen in response to the three different Cu-based forms utilized for the treatments.
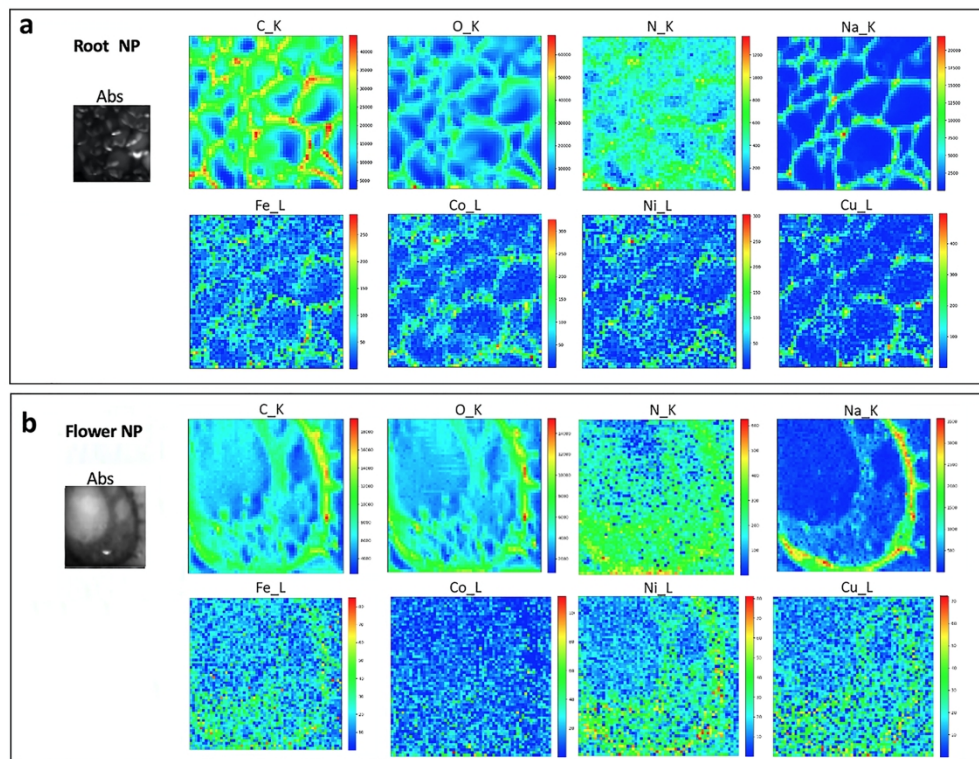
Figure 4. µ-XRF maps of (a) roots and (b) flowers from plants treated with CuO NPs. Names of the mapped elements are on top of each figure. The maps are related to the black and white square on top left (Abs) which is the 20x image of the cells in the root tissue and pollen sac tissues treated with CuO NPs. Cu map is always the last in the second row for (a) and (b).
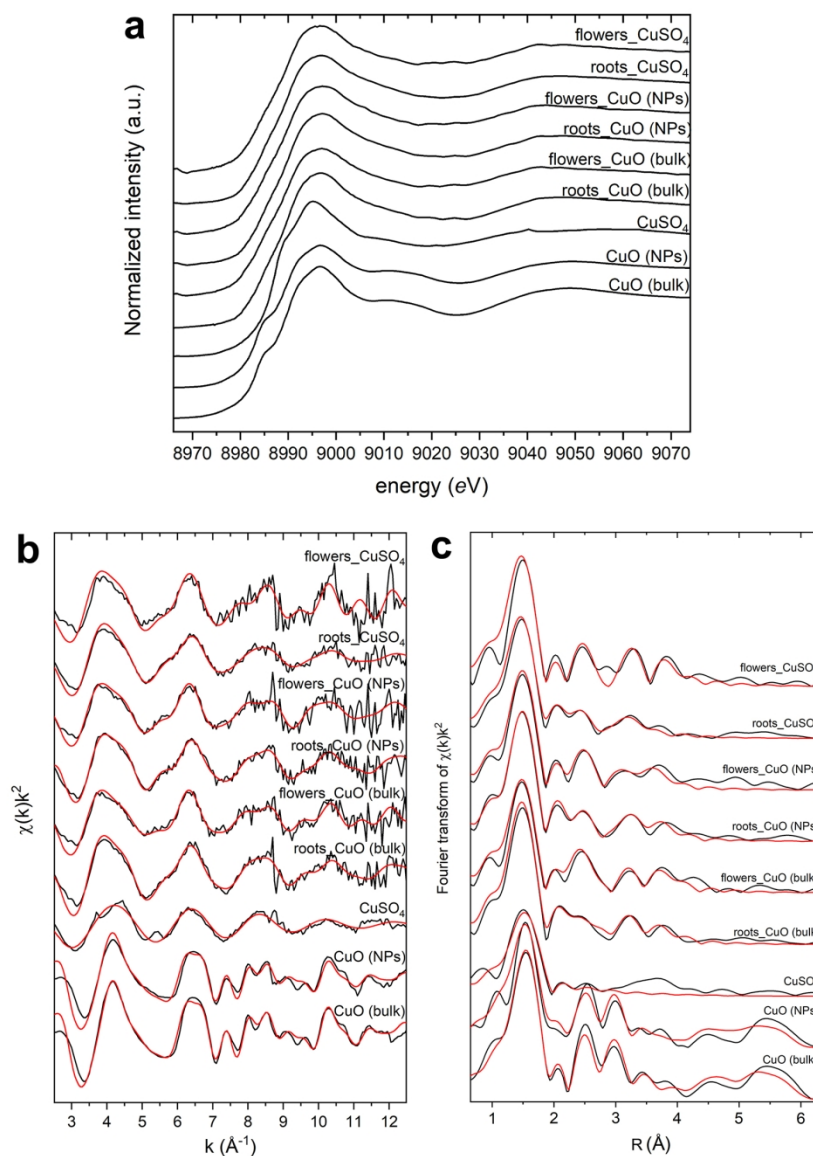
Figure 5. XANES spectra of the measured samples and model compounds (a). Cu K-edge k2-weighted EXAFS region (b) and Fourier transforms (c) of plant tissues and model compounds. Solid lines are data, red lines are fits. Energy was calibrated with a Cu reference foil (8978.9 eV). In order to minimize beam-induced damage, spectra of samples were acquired at 80 K with a constant k step of 0.05 Å-1 up to a maximum k value of 12.5 Å-1 for plant tissues while model compounds were measured at room temperature with a k step of 0.03 Å-1 up to k=18 Å-1. Plant samples were measured in the fluorescence mode with a 12-element HP-Ge detector.